A photodriven energy efficient membrane process for trace VOC removal from air: First step to a smart approach

Fabien Gérardin, Anaëlle Cloteaux, Julien Simard, Éric Favre

Version of Record: https://www.sciencedirect.com/science/article/pii/S1385894721011530
Manuscript_c97051f0ed0998888e774d8d2fa2835d

A photodriven energy efficient membrane process for trace VOC removal from air: First step to a smart approach

Fabien Gérardin[1*], Anaëlle Cloteaux[2], Julien Simard[1], Éric Favre[2]

[1] Institut National de Recherche et de Sécurité, Rue du Morvan, CS60027, 54519 Vandœuvre Cedex, France

[2] Laboratoire Réactions et Génie des Procédés, UMR 7274 CNRS Université de Lorraine, 1 rue Grandville BP20451, 54001 Nancy Cedex, France

Abstract

The VOC removal from air is a major concern both in the context of occupational and domestic exposure. Membrane processes are often presented as unsuitable for the removal of low concentrated VOCs mainly due to a too low driving force leading to high-energy costs. The aim of the work presented in this paper is to investigate the original combination of a dense membrane separation process and a photocatalytic oxidation process implemented in the permeate compartment of the system for the intensification of the separation and the decomposition of toxic compounds. An unpublished modeling of this coupled processes completed by a robust experimental study integrating the main operating parameters (flow rates, pressures, membrane materials, catalyst mass, concentration, light irradiance) is presented in this work. This exploratory study shows that for a test compound, n-hexane, this approach significantly intensifies the separation of a low-concentration VOC (i.e. 1 to 25ppm) with a low-energy cost. The model developed here allows designing more enhanced system such as hybrid plug-flow module operating with a thin polydimethylsiloxane membrane and sweep-gas on the permeate compartment. This configuration seems particularly relevant for an efficient VOC separation and limits greatly the presence of potential by-products in the treated effluent, such as formaldehyde, acetaldehyde or carbon monoxide well-known intermediates identified in photocatalysis. From a reaction position, this

hybrid process leads to the VOC photocatalytic oxidation advantageously increased compared to a single plug-flow reactor especially for low light irradiances (≈3 W m^{-2}). This process is suitable to work with the solar irradiance.

Keywords

Membrane, photocatalysis, VOC removal, modeling, energy efficiency, intensification

*__Corresponding author__: Fabien Gérardin – Fabien.gerardin@inrs.fr

1. Introduction

The technologies available for the removal of high VOCs concentrations from air are based on oxidation (thermal, catalytic) or recuperative processes (gas/liquid absorption, gas/solid adsorption, condensation, membrane separation). For the treatment of effluents with low or very low VOCs concentrations, such as indoor air, the baseline process is still adsorption on activated carbon or zeolites [1].

While it is efficient at trapping many pollutants, adsorption is a discontinuous and unsteady process leading to the progressive saturation of the adsorbent material. This generates waste or requires regeneration [2]. Moreover, the adsorption efficiency can be reduced in the presence a high concentration of water vapor [3, 4].

Technologies based on gas permeation provide an efficient solution to selectively separate concentrated gases and vapors [5-10]. The use of dense membranes does not seem to be adequate for the separation of low VOCs concentration from air [5]. The gas transport mechanisms (solution-diffusion) involved in the gas permeation process operate with a sufficiently high concentration gradient (driving force) of the compound of interest between the retentate and the permeate to obtain an acceptable separation efficiency [5,10]. The application of high pressure in the retentate side and/or reduced pressure on the permeate side increases the separation efficiency at the expense of energy cost [11,12]. Cha et al. [6] and Majumdar et al. [11] have shown that it is possible to efficiently separate very low VOCs concentration (10 to 100 ppm) from air using hollow fiber membrane modules. However, these results were obtained by applying a high vacuum on the permeate side.

The aim of the work presented in this paper is to explore the possibility of intensifying the separation of low VOCs concentration using dense polymeric membranes. The principle is based on lowering the chemical potential of the VOCs of interest in the permeate compartment. The lowering of the chemical potential can be achieved by dilution ("sweep gas or sweep liquid"), by reduced pressure or

by the removal of the compound concerned [13]. The approach presented here consists of decomposing VOC by photocatalytic oxidation, leading to partial or complete mineralization of the compound. Thus, the coupling of gas permeation and VOC photocatalytic decomposition should enhance VOC separation from the air and decomposition into low toxic compounds (H_2O, CO_2, N_2) [14]. Photocatalysis is adapted for decomposing low-concentration substances [14-15]. Photocatalysis is an advanced oxidation process based on the absorption of light energy by a photocatalyst. Photo-induced redox reactions in the presence of water and atmospheric oxygen lead to the formation of highly reactive molecules, mostly free radicals such as hydroxyl radicals. These radicals participate in the decomposition of various organic and inorganic substances present in the effluent [15, 16]. Currently, the semiconductor (photocatalyst) used in most applications is titanium dioxide (TiO_2). In this case, the spectral range concerned by the photocatalytic properties is mostly UV ($\lambda < 388$ nm) [14]. Photocatalysis operates at ambient temperature and atmospheric pressure with a reasonable energy cost [14]. A recent review indicates that the work dedicated to the decomposition of VOCs is significant from an engineering point of view as well as for the development of photocatalytic materials[17, 18]. For example, some photocatalysts based on gallium oxide (Ga_2O_3), tungsten oxide (WO_3) or bismuth oxyhalide (BiOI) present promising performances [19-21]. Other approaches consist in improving the performance of TiO_2 by metal doping with platinum, manganese or silver [22].

Many air treatment systems based on catalytic, photocatalytic or non-thermal plasma oxidation operate without any prior separation step. By design, these systems often lead to incomplete decomposition of the targeted pollutants and could generate toxic reaction intermediates [23,24]. The principle of the hybrid process presented here should also allow a reduction in the presence of possible by-products of photocatalytic decomposition in the treated effluent.

The coupling of a gas separation process using non-porous membranes and a photocatalytic process in the same device can be considered as a membrane reactor [25-27]. In many configurations, the

membrane is the reactor, in other cases, the membrane is the catalyst [27,28]. The research described in the literature indicates that for gas permeation, the permeate side of a membrane reactor is rarely considered a reaction space. When it is not integrated into the membrane, the catalyst is systematically placed in the retentate space or on the surface of the membrane on the retentate side. The most commonly observed configuration of a membrane reactor is therefore a reaction followed by separation and not the separation step followed by reaction. This observation is supported by a recent literature review by Qing et al. [29] which focuses more specifically on reaction/separation couplings with polymeric catalytic membranes.

Photocatalysts, mainly the anatase form of TiO_2 and more rarely zinc oxide (ZnO), have been used on the surface or in membranes and are systematically arranged on the retentate side [30]. Membranes identified in the literature are exclusively porous membranes [30-32]. The main published works that study the photocatalysis/membrane separation coupling concern the pervaporation or removal of pollutants in the liquid phase [12, 33]. However, Tusuru et al. [34,35] and Maira et al. [36] have studied the photocatalytic decomposition of VOCs in the gas phase with porous membranes. In the latter case, the catalyst is also located in the retentate compartment of the membrane module.

The main conclusion of the literature review on the coupling of chemical reactions and a membrane in a reactor is that membranes are systematically used to intensify the reaction process on the retentate side. The novelty of the work presented in this paper is the integrated concept of membrane separation / photocatalytic reaction for trace VOC removal. More specifically, there is little or no mention in the literature of a membrane reactor combining a dense membrane and a photocatalyst located in the permeate compartment; a very limited number of studies report different approaches such as light switchable porous membrane materials or photomechanical energy conversion systems [37, 38]. The permeate photocatalysis option offers the unique opportunity to in situ generate the permeant transmembrane driving force. No compression or

vacuum pumping should be, in principle needed, the process being photodriven. Consequently, improvements in terms of energy efficiency can be expected, and will be investigated hereafter.

In summary, the study presented in this paper focuses on the coupling of gas permeation using a dense polymeric membrane and a photocatalytic process placed in the permeate compartment of a flat membrane module (Figure 1). The influence of parameters on the operation of the system (such as feed flow rate, pressure, VOC concentration and membrane type and light irradiance) has been experimentally evaluated. A modeling of the different processes that take part in this coupling is conducted. Finally, for exploratory purposes, the modeling of a hybrid module operating in plug flow/plug flow configuration is also presented. The proof of concept study was conducted for a single VOC: n-hexane. This compound belongs to the aliphatic hydrocarbons and its photocatalytic decomposition is known [39, 40]. The corresponding kinetics is rather well adapted to Langmuir hinshelwood monomolecular model [39]. Moreover, the literature indicates that the photocatalytic oxidation of this compound does not produce catalyst poisoning, which is convenient for a preliminary study.

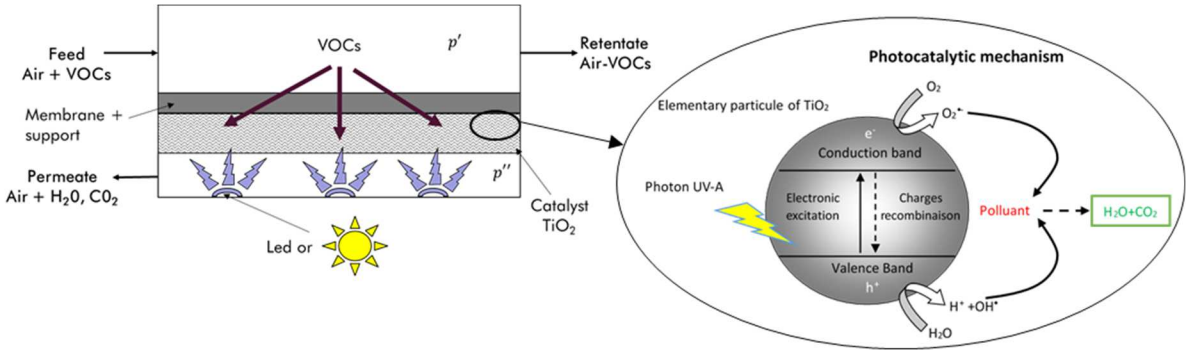

Figure 1 Principle of coupling of gas permeation and photocatalytic reaction on the permeate side

2. Materials and method

2.1. Experiment

The work was carried out with a system for generating air-VOC or nitrogen-VOC mixtures (Figure 2). A flat membrane module is associated with the generation system. This experimental bench is

equipped with a control system for concentrations, flow rates, pressures, temperature and relative humidity. The air-VOC mixture is produced from gas bottles, the VOC concentration of which is calibrated.

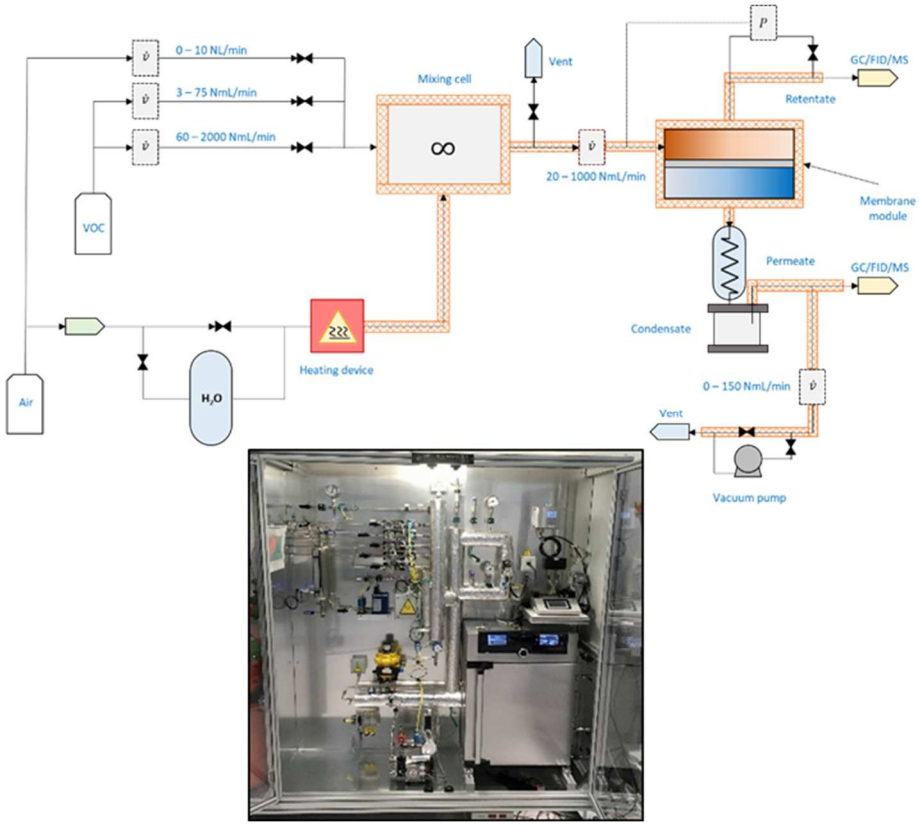

Figure 2 Experimental gas permeation setup

The analysis of VOCs in the retentate and permeate fluxes is performed online by a PerkinElmer system coupling a thermodesorber (TurboMatrix 100), a gas chromatograph (Clarus 580) equipped respectively with a flame ionization detector and a quadrupole mass spectrometer (Clarus SQ 8). The mineralization yield of n-hexane is determined by measuring the CO_2 concentration at the output of the retentate and permeate compartments by gas chromatography and a pulsed discharge ionization detector. UV-A irradiance was measured with a light detector (Gigahertz Optik radiometer model X11-XD-9511, range 315/400 nm).

2.1.1. Description of the hybrid membrane - photocatalysis experimental system

The experimental coupling device developed in this study corresponds to the configuration presented in Figure 1. The flat module works with the implementation of the photocatalyst in the permeate compartment. The compartment, in which three LEDs (LED Engin - LZ1-00U600 - 5W) are placed with a spectral peak centered on 365 nm, is separated from the permeate compartment by borosilicate glass. The LEDs illuminate the photocatalyst with an irradiance ranging from 0.03 to 30 W m^{-2}. The retentate and permeate spaces are considered to be continuous stirred-tank reactors (CSTR). The retentate and permeate volumes are 65 mL and 145 mL respectively. The range of membrane surface area is 12.5 - 50 cm^2. The module is fed with a flow rate of a few mL min^{-1} to 1000 mL min^{-1}. The pressure range on the retentate side is 1.2 - 6 bar. The minimum permeate pressure is 0.1 bar. The concentration range for each VOC that can be used is a few dozen ppb to 5000 ppm.

The photocatalyst is Quartzel® photocatalytic felt, supplied by Saint-Gobain Quartz (France), which is made from entangled 8-12 µm diameter Quartz fibers coated by sol-gel TiO_2-anatase. It has a total surface density of 120 g m^{-2}, including 40 g m^{-2} of TiO_2, so that one single layer of Quartzel© photocatalytic felt had a TiO_2 amount of 4 mg cm^{-3}, also expressed as a TiO_2 surface density of 4 mg cm^{-2}. The medium porosity is estimated to be = 0.995.

Two kinds of dense membranes have been used in this study. The first membrane is a 50 µm thick PDMS (Goodfellow®) rubbery polymeric membrane without support. PDMS membranes indeed show high selectivity for many VOCs with respect to N_2 and O_2 [9, 41-43]. The second membrane is a rubbery polymer thin-film composite membrane, with the polyethylene oxide containing block copolymer PolyActive as selective layer, a PDMS protective layer and a porous support in polyacrylonitrile (PAN) [44]. PolyActive membranes are very often used for CO_2 separation. A remarkable feature of this membrane is the high CO_2/N_2 selectivity at relatively high CO_2 permeance, which is a favorable characteristic for an efficient membrane application. Moreover, this kind of membrane presents permeabilities that allow the separation of many VOCs from air [45].

The influence parameters studied are the VOC concentration, the retentate and permeate pressure, the membrane thickness, the catalyst mass and the catalyst illumination intensity.

The operating conditions are:

- Membranes: PolyActive and PDMS - 50 µm
- Membrane diameter 70 mm (membrane effective surface area = 38.5 cm^2)
- VOC inlet concentration: 1, 5, 10 and 25 ppm n-hexane
- Feed flow rate: 50 and 100 NmL min^{-1}, i.e. 3.71x10^{-5} mol s^{-1} and 7.42x10^{-5} mol s^{-1}
- Pressure (*p''*: permeate pressure/*p'*: retentate pressure): 0.98 bar/1.2 bar - 0.98 bar/2 bar - 0.98 bar/3 bar - 0.5 bar/2 bar;
- Temperature: 24°C;
- Relative humidity: 1% (in the feed flow);
- Irradiance: 0.04, 0.3, 1.2, 2.8, 7 and 11 W m^{-2};
- Catalyst mass: *m1*=0.15 and *m2*=0.41 g

2.1.2. Kinetics of photocatalytic decomposition of n-hexane

The photocatalytic decomposition of n-hexane has already been studied [39,40]. The production of highly oxidative OH˙ radicals by the light activation of TiO_2 leads to the photocatalytic oxidation of this compound according to the equation (1) :

$$C_6H_{14} + \frac{19}{2}O_2 \xrightarrow{TiO_2,h\nu} 6CO_2 + 7H_2O \qquad (1)$$

The kinetic model proposed by the authors is a Langmuir-Hinshelwood monomolecular model for a given irradiance and catalyst mass [39]. The kinetic model proposed in this study is a Langmuir-Hinshelwood model that integrates the light intensity absorbed by the catalyst and the mass of the photocatalytic medium. The proposed model is:

$$r = mI_{abs}^{n_i}\frac{kKC}{1+KC} = mI_{abs}^{n_i}\frac{kKx(\frac{P}{RT})}{1+Kx(\frac{P}{RT})} \qquad (2)$$

With *r* for the reaction rate (mol s^{-1}), *m* for the mass of photocatalytic medium (g), I_{abs} for the light power absorbed by the photocatalytic medium ((Wm^{-2})^{ni}), n_i is the order with respect to I_{abs}, *k* is the apparent kinetic constant (mol m^{-3} ($W\ m^{-2}$)$^{-ni}$ g^{-1} s^{-1}), *K* is the adsorption constant ($m^3\ mol^{-1}$) and *C* is the concentration of n-hexane in the reactor (mol m^{-3}). The reaction rate is also expressed with *x* as the mole fraction of n-hexane, *R* as the ideal gas constant (J mol^{-1} K^{-1}), *T* as the temperature (K) and *P* as the pressure (Pa). The kinetic study was conducted with a CSTR.

The light intensity absorbed by the photocatalytic medium was measured as a function of the thickness of the medium. The light absorption model is:

$$I_{abs} = I_0\left(1 - e^{(-\alpha l)}\right) \qquad (3)$$

with I_0 for the irradiance received by the photocatalytic medium (W m^{-2}), α the absorption coefficient (m^{-1}) and *l* the thickness of the photocatalytic medium (m).

2.1.3. Characterization of hybrid system

In addition to the hydrodynamic behavior of the retentate and permeate compartments of the system, the operation of the membrane module shown in Figure 3 is characterized by the following parameters:

- The driving force which represents the ratio of the pressures on the permeate and retentate sides:

$$\psi = \frac{P''}{P'} \qquad (4)$$

- The stage cut (%), which is the ratio of the total permeate flow rate to the feed flow rate:

$$\theta = \frac{Q_p}{Q_{in}} \times 100 \qquad (5)$$

- The recovery ratio of n-hexane (%):

$$R_{hex} = 1 - \frac{Q_r x_{r_{hex}}}{Q_{in} x_{in_{hex}}} \times 100 \qquad (6)$$

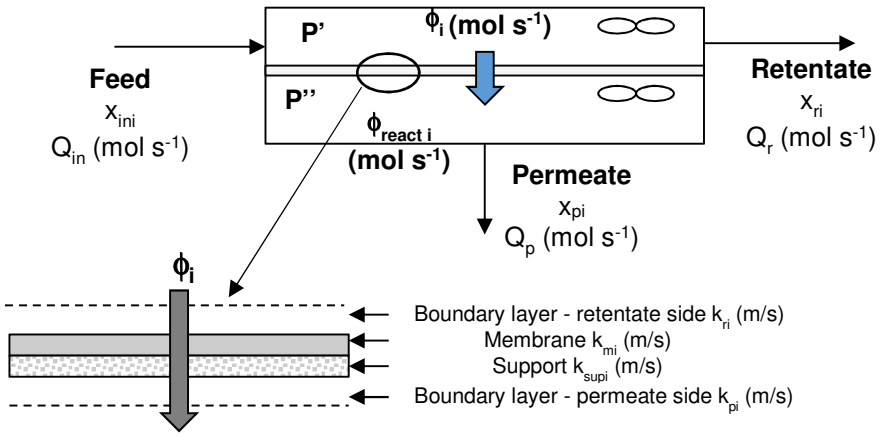

Figure 3 Schematic representation of the experimental module and the different layers of the membrane system

In Figure 3, x_{ini}, x_{ri} and x_{pi} correspond respectively to the mole fractions of compound *i* in feed, retentate and permeate compartments. Q_{in}, Q_r and Q_p are the molar fluxes in feed, on the retentate and permeate side, respectively. ϕ_i is the flux of compound *i* through the membrane (mol s^{-1}) and $\phi_{react\ i}$ is the reaction flux of compound *i* (mol s^{-1}).

The photocatalytic reaction is a heterogeneous process that requires the introduction of criterion fe defined by equation (7). This criterion indicates whether the decomposition process of n-hexane in the permeate compartment is limited by the chemical reaction or by the external diffusion of the compound from the bulk to the fibers of the photocatalytic medium. It is assumed that the internal transport of the compound into the TiO_2 particule is not limiting. Given the very low flow velocities in the permeate compartment, the transport process of n-hexane to the photocatalytic fibers is considered to be diffusive and non-convective.

$$fe = \frac{\bar{r}L^2}{V_r D_m C_{p\ hex}} = \frac{\bar{r}L^2}{V_r D_m x_{p\ hex}(\frac{p''}{RT})} \qquad (7)$$

with $\bar{r}$ for the apparent decomposition rate in the permeate compartment (mol s^{-1}), V_r for the volume of the photocatalytic medium (m^3), L characterized by V_c/A_c, where V_c and A_c are respectively the specific volume of the catalytic fibers (m^3 g^{-1}) and the specific surface area of the catalytic fibers (m^2 g^{-1}), and D_m for the molecular diffusion coefficient of n-hexane (m^2 s^{-1}). $C_{p\ hex}$ and $x_{p\ hex}$ are

respectively the concentration (mol m^{-3}) and the hexane mole fraction in the permeate compartment. Thus, if *fe* <<1, the decomposition process will take place according to a chemical regime, whereas if *fe*>>1, the process will operate according to a diffusional regime.

The principle of coupling of a membrane separation process and a reaction process requires the introduction of a second criterion, *fe'*, defined by equation (8). This criterion compares the maximum reaction rate and the maximum flux of VOC through the membrane.

$$fe' = \frac{Maximal\ reaction\ rate}{Maximal\ VOC\ flux\ trough\ membrane+support} = \frac{r_{max}}{\phi_{i\,max}} \qquad (8)$$

This criterion is used to determine the operating mode of the hybrid system. The limiting process can be either the reaction process (*fe'*<1) or the process of n-hexane transport through the membrane (*fe'*>1).

The mineralization of n-hexane by the photocatalytic reaction is characterized by a mineralization yield (%) defined by equation (9):

$$R_{CO2} = \frac{\emptyset_{CO_2}}{6\times\emptyset_{reac\ hexane}} \times 100 = \frac{\emptyset_{CO_2}}{6\times r} \qquad (9)$$

where

$$\emptyset_{CO_2} = Q_r \times x_{r\,CO2} + Q_p \times x_{p\,CO2} - Q_{in} \times x_{in\,CO2} \qquad (10)$$

2.2. Modeling

2.2.1. Modeling of the experimental module

This section is dedicated to the modeling of the experimental system for an effluent composed of *n*=5 compounds: nitrogen, oxygen, n-hexane, water and carbon dioxide. The photocatalytic reaction is considered in the permeate compartment. The following assumptions are made:

- Retentate and permeate compartments are CSTRs;

- Constant permeability for each compound;

- Steady state of the various phenomena;

- Isothermal conditions of the studied system;

- Uniform thickness of the membrane;

- Constant pressure in each compartment of the module.

The different processes are modeled based on the molar balances and the expressions of the molar fluxes through the membrane.

Overall molar balance

$$Q_{in} = Q_r + Q_p + \sum_{i=1}^{n} \phi_{react\,i} \quad (11)$$

Overall molar balance for each compound *i*

$$Q_{in} x_{in\,i} = Q_r x_{ri} + Q_p x_{pi} + \phi_{react\,i} \quad (12)$$

Molar flux through the membrane for each compound *i*

$$\phi_i = \frac{SP_i}{z}\left[P' x_{r\,i} - P'' x_{pi}\right] \quad (13)$$

And

$$x_{p\,i} = \frac{\phi_i - \phi_{react\,i}}{\sum_{i=1}^{n}(\phi_i - \phi_{react\,i})} \quad (14)$$

$$\sum_{i=1}^{n} x_{pi} = 1 \quad (15)$$

$$\sum_{i=1}^{n} x_{ri} = 1 \quad (16$$

$$\phi_{react\,i} = \nu_i r \quad (17)$$

$\phi_{react\,i}$ can be positive or negative depending on whether it is a compound that disappears or appears. *S* and *z* are the surface area (m^2) and thickness (m) of the membrane, respectively. *Pi* is the membrane permeability of the compound *i* (Barrer or mol m^{-1} s^{-1} Pa^{-1}). ν_i is the stoichiometric coefficient of compound *i* from equation (1).

ϕ_i is expressed by taking into account the different resistances, in particular those of the laminar mass transfer boundary layers on either side of the membrane (Figure 3):

$$\phi_i = K_i S\left[C_{ri} - C_{pi}\right] = S\frac{\left[C_{ri} - C_{pi}\right]}{\frac{1}{k_{ri}} + \frac{1}{k_{mi}} + \frac{1}{k_{supi}} + \frac{1}{k_{pi}}} \quad (18)$$

$$\frac{1}{K_i} = \frac{1}{k_{ri}} + \frac{1}{k_{mi}} + \frac{1}{k_{supi}} + \frac{1}{k_{pi}} \qquad (19)$$

K_i (m s^{-1}) represents the overall mass transfer resistance or overall mass transfer coefficient of compound *i* through the membrane.

In some cases, for example when the permeability of a compound is very high, a concentration gradient may appear at its boundary layer on the retentate side. This phenomenon, named concentration polarization, results in a decrease in the separation efficiency of the membrane for this compound. It is generally accepted that there is no concentration gradient on the permeate side [5]. However, if a sweep gas is applied on the permeate side or, as in the present case, a reaction takes place in this compartment, it is likely that a concentration gradient will appear in the boundary layer on the permeate side.

Thus, it is important to integrate the phenomenon of concentration polarization into the model on both membrane sides using equations (20) and (21).

- Retentate side

$$SD_{i\_r} \frac{dx_{ri_{BL}}}{d\delta_r} = Q_p(x_{ri} - x_{ri_{BL}}) \times \frac{RT}{P'} \qquad (20)$$

For δ_r=0, $x_{ri_{BL}} = x_{ri_0}$ and for δ_r=δ_R , $x_{ri_{BL}} = x_{ri}$

- Permeate side

$$SD_{i\_p} \frac{dx_{pi_{BL}}}{d\delta_p} = -Q_p(x_{pi_{BL}} - x_{pi}) \times \frac{RT}{P''} \qquad (21)$$

for δ_p=0, $x_{pi_{BL}} = x_{pi_0}$ and for δ_p=δ_P, $x_{pi_{BL}} = x_{pi}$

with D_{i_r} and D_{i_p} (m^2 s^{-1}) respectively for the molecular diffusion coefficients of compound *i* on the retentate and permeate sides. δ_r and δ_p (m) represent the thickness of the boundary layers on the surface of the membrane on the retentate and permeate sides. $x_{ri_{BL}}$ and $x_{pi_{BL}}$correspond to the mole fractions of compound i in each boundary layer.

2.2.2. Modeling of a hybrid system operating in countercurrent plug flow mode

An integrated photodriven system operating in countercurrent plug flow (PF) mode is described in Figure 4. The modeling of this system is carried out for an effluent composed of *n*=5 compounds: nitrogen, oxygen, n-hexane, water and carbon dioxide. The catalyst, which is placed in the permeate compartment, is illuminated by homogeneous UV-A radiation. The modeling is performed for a hybrid module which contains a membrane with a 3.5 µm thick active layer of PDMS and the catalyst *m1*. The number of cells in the model is n_c=10. The effluent that feeds the module is a mixture of air and n-hexane, the concentration of which is C_{in}=10 ppm. The feed rate is Q_{in}=100 NmL min^{-1}. A gas sweep flow rate can also feed the permeate compartment. The countercurrent plug flow configuration is the conservation of a concentration gradient of compound i along the module which leads to a higher separation efficiency than for a CSTR/CSTR system. Furthermore, a plug flow reactor often increases the decomposition yield compared to a CSTR.

In this model, the assumptions are:

- Constant permeability for each compound;
- Steady-state regime of the various phenomena;
- Isothermal conditions of the system studied;
- Uniform thickness of the membrane;
- Constant pressure in each compartment of the module.

The differential molar balances are written in steady-state conditions with respect to *S* (Figure 4):

$$\frac{dq'}{ds} = -\sum_{i=1}^{n} \emptyset_i(x_{ri}, x_{pi}, P', P") \quad (22)$$

$$\frac{dx_{ri}}{ds} = \frac{x_{ri}\sum_{i=1}^{n}(\emptyset_i(x_{ri},x_{pi},P',P")-\emptyset_i(x_i,y_i,P',P"))}{q'} \quad (23)$$

$$\frac{dq"}{ds} = -\sum_{i=1}^{n}(\emptyset_i(x_{ri}, x_{pi}, P', P") - \phi_{react\ i}) \quad (24)$$

$$\frac{dx_{pi}}{ds} = \frac{(x_{pi}\sum_{i=1}^{n}(\emptyset_i(x_{ri},x_{pi},P',P")-\phi_{react\ i}))-(\emptyset_i(x_{ri},x_{pi},P',P")-\phi_{react\ i})}{q"} \quad (25)$$

Initial conditions: for *S*=0, $q'=Q_{in}$, q''= unknown, x_{ri} = unknown and y_{ri} = unknown

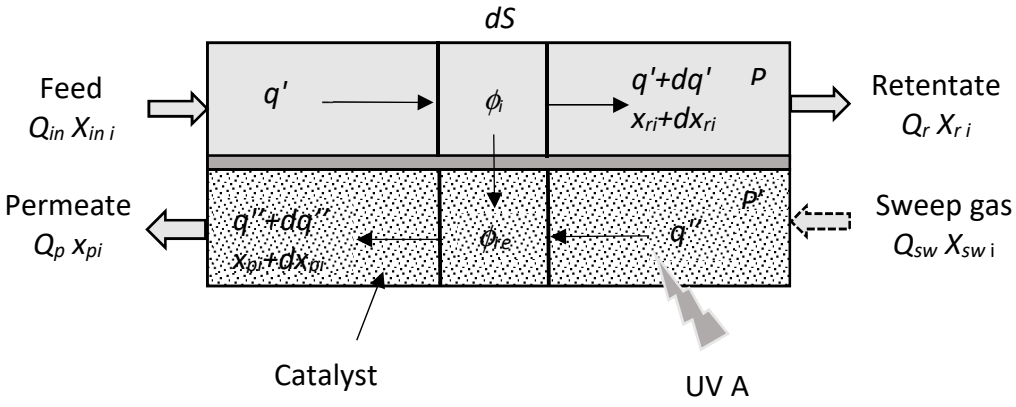

Figure 4 Description and differential molar balance for a countercurrent plug flow hybrid system

A system of non-linear first-order differential equations has thus to be solved. Usually, this kind of differential system is solved by the 4th order Runge Kutta-Fehlberg method [46]. Here, however, given that some initial conditions are unknown, this method can only be applied if one estimates the unknown initial conditions using the shooting technique, which for a problem with n compounds becomes complex and laborious.

The problem can be solved by discretizing the membrane module using the finite difference method [47,48]. This is equivalent to dividing the module into n_c cells (Figure 5) with a membrane surface area $\Delta S=S/n_c$ (m^2) and a catalyst mass $\Delta m=m/n_c$.

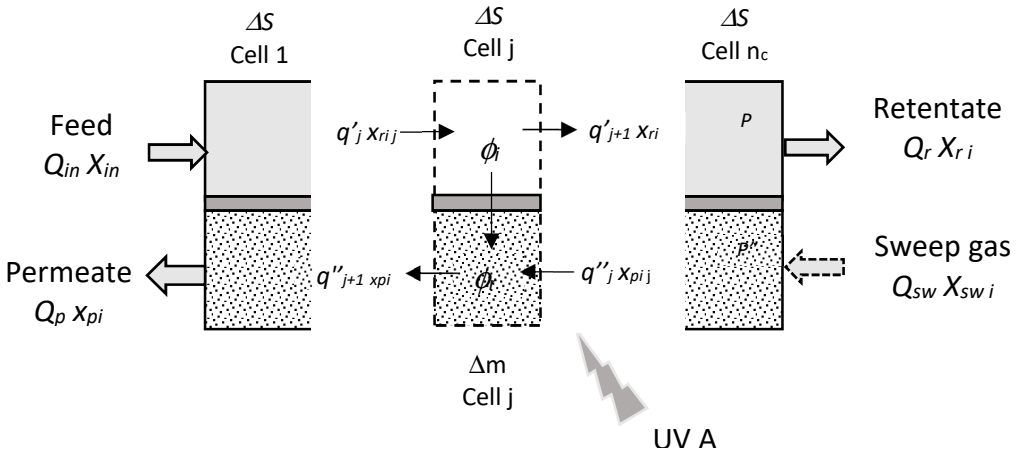

Figure 5 Finite difference discretizations for countercurrent plug flow configuration

Each *j* cell of the module is a CSTR. Molar balances are performed on each cell according to:

Overall molar balance

$$q'_j + q''_{j+1} = q''_j + q'_{j+1} \qquad (26)$$

Local molar balance (for each compound)

$$q'_j x_{ri\,j} + q''_{j+1} x_{pi\,j+1} = q''_j x_{pi\,j} + q'_{j+1} x_{ri\,j+1} \quad (27)$$

Transport equation

$$q''_j x_{pi\,j} = \Delta S \emptyset_{i\,j} + q''_{j+1} x_{pi\,j+1} \quad (28)$$

Sums of mole fractions

$$\sum_{i=1}^{n} x_{ri\,j} = 1 \quad (29)$$

$$\sum_{i=1}^{n} x_{pi\,j} = 1 \quad (30)$$

The mass balances lead to a system of n_c * (2+2*n) non-linear algebraic equations which is solved using the fsolve solver of the MATLAB© software.

2.2.3. Modeling of single photocatalytic plug flow reactor

The modeling of a photocatalytic reactor operating in plug-flow mode is represented by equation (31). This modeling is used to compare the n-hexane removal performance of this type of reactor with that of a hybrid module described in the previous section.

$$\int_{x_{in}}^{x_{out}} dx = \frac{1}{Q_{in}} \int_0^m -r dm = \frac{1}{Q_{in}} \int_0^m -I_{abs}^{n_i} \frac{kKx(\frac{P}{RT})}{1+Kx(\frac{P}{RT})} dm \quad (31)$$

3. Results and discussion

3.1. Kinetics of photocatalytic decomposition of n-hexane

The kinetic model proposed in this study is a Langmuir-Hinshelwood model. The model integrates the mass of the photocatalytic medium and the light intensity absorbed by the catalyst (equation (2)). The parameters of this model have been defined experimentally.

$$r = m I_{abs}^{n_i} \frac{kKC}{1+KC} \quad (2)$$

where n_i =0.65, k=1.9x 10^{-6} mol m^{-3} (W m^{-2})$^{-0.65}$ g^{-1} s^{-1}, K=3.7 x 10^4 m^3 mol^{-1}.

The light intensity absorbed by the catalyst follows a law of kind:

$$I_{abs} = I_0\left(1 - e^{(-\alpha l)}\right) \quad (3)$$

α is determined experimentally, for the photocatalyst used α= 76. The photocatalytic media used in the study have a mass of *m1*=0.15 g and *m2*=0.41 g and a thickness *l* of 0.005 m and 0.015 m respectively.

This criterion *fe* defined equation (7) indicates whether the decomposition process of n-hexane in the permeate compartment is limited by the chemical reaction or by the external diffusion of the compound from the bulk to the fibers of the photocatalytic medium. The specific volume of the photocatalytic fibers V_c= 6.4x10-7 m^3 g^{-1} and the corresponding specific surface area A_c=120 m^2 g^{-1}. The molecular diffusion coefficient of n-hexane D_m=8x10-6 m^2 s^{-1}. In this study, for all cases presented, *fe*<<1. This means that the decomposition process is limited in the permeate compartment by chemical rate.

3.2. Coupling of membrane separation and photocatalytic oxidation in the experimental module

For convenience, concentrations are expressed in this part of the document in ppm. The results presented correspond to experiments and modeling performed with the experimental module. The surface area PolyActive membrane is *S*=38.5 cm^2. Figure 6 represents the evolution of the n-hexane recovery ratio and the corresponding concentrations versus the absorbed light intensity for Q_{in}= 50 NmL min^{-1} i.e. 3.71x10^{-5} mol s^{-1}, *P'*=2 bar and *P''*=0.98 bar and with the catalyst masses *m1* and *m2* (Figure 6 a,b). For this case, the maximum recovery ratio is close to 70% and the corresponding stage cut, θ is 17%.

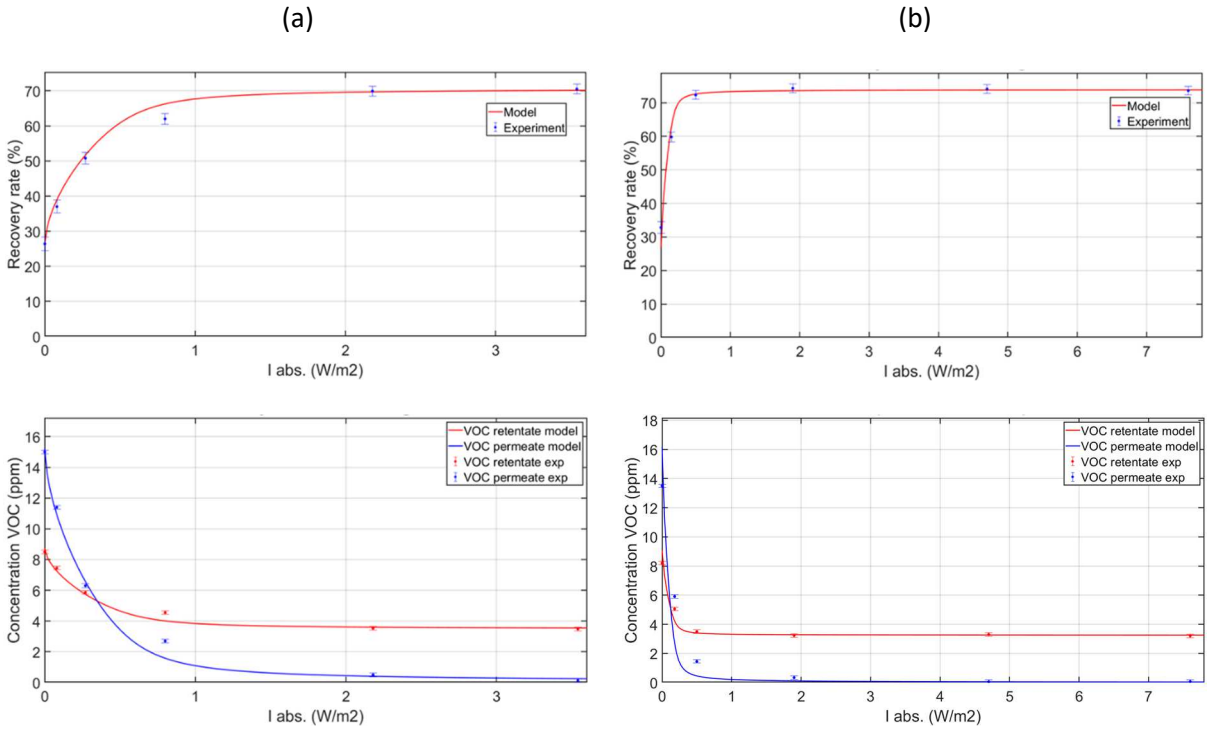

Figure 6 n-hexane recovery ratio and n-hexane retentate and permeate concentrations vs I_{abs} for catalyst masses *m1* (a) and *m2* (b) - C_{in}=10 ppm - Q_{in}=50 NmL min^{-1} -$\psi = 0.98/2$

Figure 7 represents the same parameters as those presented in Figure 6 for Q_{in}= 100 NmL min^{-1} i.e. 7.42x10^{-5} mol s^{-1}. It is very clear that the recovery ratio of n-hexane increases significantly when n-hexane is decomposed in the permeate compartment. Indeed, the higher the light intensity absorbed by the catalyst, implying a high decomposition rate, the higher the removal rate. For example, for the case shown in Figure 7, the removal rate of the initial n-hexane, i.e. without chemical reaction, is about 15% and reaches a maximum value of 55%; the stage cut is θ=8.5%, the enhancement factor (*EF*) defined according to equation (32) is 3.7.

$$EF = \frac{R_{hex\,Max}}{R_{hex\,0}} \qquad (32)$$

with $R_{hex\,Max}$ for the maximum recovery ratio of n-hexane (%) and $R_{hex\,0}$, for the recovery ratio of n-hexane (%) with I_{abs} =0 W m^{-2}.

Nevertheless, for any configurations presented in Figures 6 and 7, the recovery ratio reaches a maximum value which is independent of I_{abs}. The maximum recovery ratio is the same for both

catalyst masses. This does not depend on the catalyst mass. In the process implemented here, two processes are coupled: the separation process and the reaction process. The results indicate that three operating regimes are successive when I_{abs} increases. First, there is a chemical regime which means that the rate of n-hexane removal is controlled by the chemical reaction. When the maximum recovery rate is reached, this means that the separative process becomes the limiting process and the operating regime becomes diffusional. Between these two regimes, an intermediate regime appears, which provides the transition. The maximum recovery ratio is the same for both catalyst masses. This does not depend on the catalyst mass.

(a) (b)

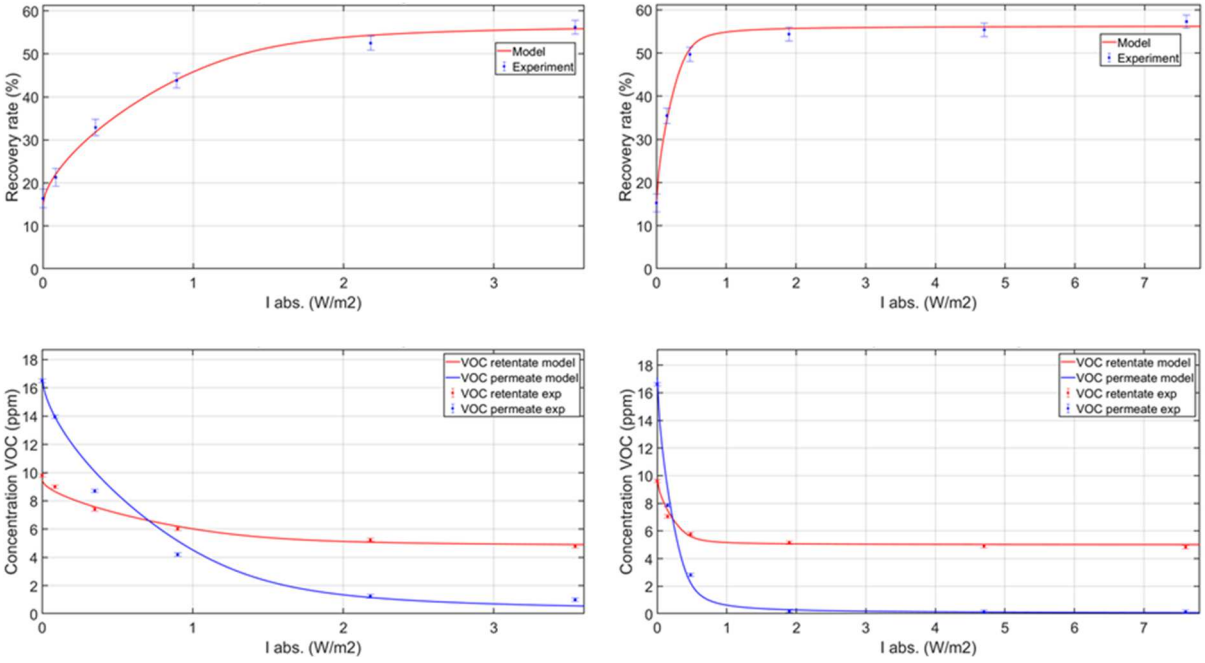

Figure 7 n-hexane recovery ratio and n-hexane retentate/permeate concentrations vs I_{abs} for catalyst masses *m1* (a) and *m2* (b) - C_{in}=10 ppm - Q_{in}=100 NmL min^{-1} - $\psi = 0.98/2$

The criterion *fe'*, defined in equations 8 and 33, is used to determine the operating regime of the process. Figure 8 represents the evolution of *fe'* as a function of I_{abs} for the operating conditions corresponding to those of the results presented in Figures 6 and 7. Thus, the transition between the chemical regime and the diffusional regime, i.e. *fe'*>1, occurs for relatively low I_{abs} values, about 0.1-0.2 w m^{-2} for the experiments carried out with a catalyst mass *m2*=0.41 g. On the other hand, for

experiments conducted with catalyst *m1*=0.15 g, the change in regime appears for significantly higher I_{abs} values.

$$fe' = \frac{r_{max}}{\emptyset_{hex\,max}} = \frac{mI_{abs}^{n_i}\frac{kKC_{r\,hex}}{1+KC_{r\,hex}}}{K_{hex}SC_{r\,hex}} \qquad (33)$$

Thus, when the system operates in a diffusional regime, the maximum recovery ratio of the compound of interest can be achieved by using a lower catalyst mass and a higher irradiance or conversely by using a higher catalyst mass and a lower irradiance. It is important to mention that when mass transfer through the membrane becomes the limiting parameter of the process, increasing the surface area of the membrane or choosing a membrane that is more permeable to the studied VOC under can allow a significant increase in the recovery rate.

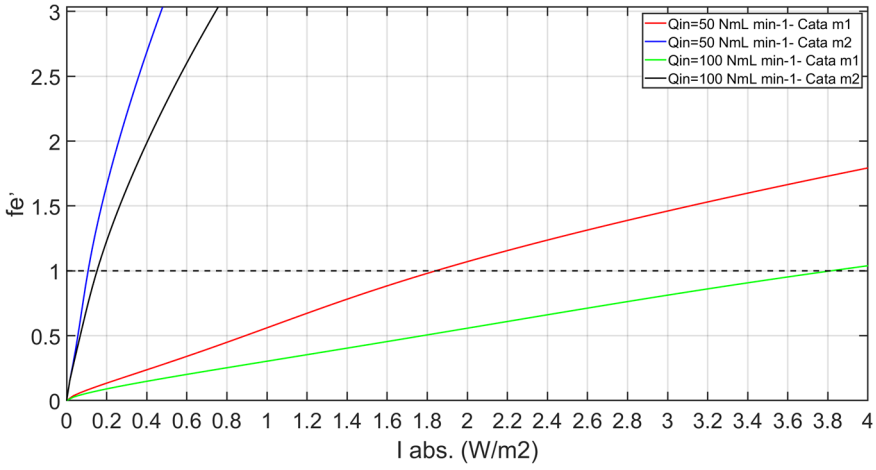

Figure 8 Representation of the *fe'* criterion vs I_{abs} - C_{in}=10 ppm - $\psi = 0.98/2$ – PolyActive membrane

The measured and modeled stage cuts for the experiments presented are close to 18% and 9% for Q_{in}=50 NmL min^{-1} and 100 NmL min^{-1} respectively (Table 1). The overall mass transfer coefficient for each compound is determined from the experimental results (Table 1).

$\psi = 0.98/2$	K_{hex} (m s^{-1})	K_{N2} (m s^{-1})	K_{O2} (m s^{-1})	K_{CO2} (m s^{-1})	K_{H20} (m s^{-1})	θ_{exp} (%)	θ_{mod} (%)
Q_{in}=50 NmL min^{-1}	2.4x10^{-4}	3.0x10^{-5}	8.1x10^{-5}	1.0x10^{-4}	6x10^{-3}	17.1	17.0
Q_{in}=100 NmL min^{-1}	2.9x10^{-4}	3.0x10^{-5}	8.1x10^{-5}	1.3x10^{-4}	6x10^{-3}	8.9	8.5

Table 1 Overall mass transfer coefficients of compounds - experimental and modeled stage cuts for the PolyActive membrane

Figure 9 shows the modeling of the evolution of the n-hexane concentration in the vicinity of the membrane on the retentate and permeate sides for given boundary layer thicknesses. These layer thicknesses were assessed from the membrane module design. On the permeate side, the thickness corresponds to the distance between the membrane support and the catalyst, i.e. 0.01 m. When observed, the concentration polarization generally appears on the retentate side of the membrane [5]. On the other hand, it is considered that there is no polarization on the permeate side except when a sweep gas is used [5]. In the case of a hybrid system such as the one presented here, with a reaction process that represents a well for the disappearance of n-hexane, it is very likely that a concentration gradient appears in the boundary layer. The modeling confirms that for C_{in}=10 ppm, Q_{in}=100 NmL min^{-1}, ψ=0.98/2 and for a catalyst mass *m2*=0.41 g, a concentration polarization is established on this side of the membrane (Figure 9). This phenomenon is not observed in the boundary layer on the retentate side and the overall transfer coefficient K_{hex} does not vary a lot with different hydrodynamic conditions (Table 1).

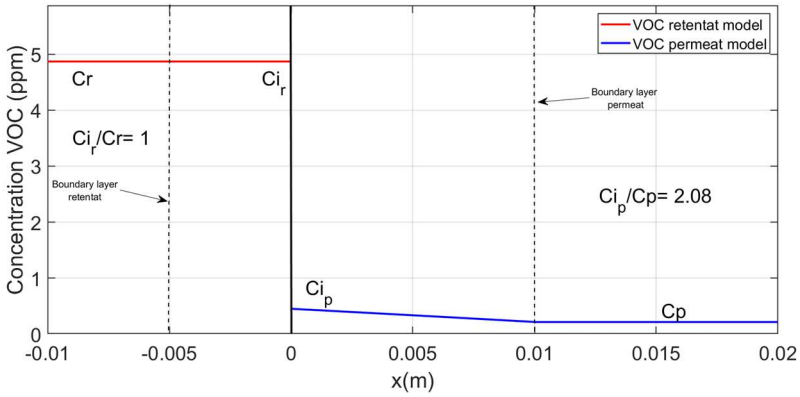

Figure 9 Representation of the concentration polarization for n-hexane - C_{in}=10 ppm - Q_{in}=100 NmL min^{-1} - $\psi = 0.98/2$ - Catalyst *m2* – I_{abs} =7.5 W m^{-2}

Figure 10 presents an example of the n-hexane recovery ratio vs I_{abs} for processes implemented separately or coupled, i.e.:

- Photocatalytic decomposition in the experimental module without membrane (CSTR);
- Membrane separation of n-hexane without photocatalytic oxidation;
- Coupling membrane separation and photocatalytic oxidation in the permeate compartment of the experimental module.

The corresponding operating conditions are C_{in}=10 ppm, Q_{in}=100 NmL min^{-1}, ψ=0.98/2, catalyst *m1* and PolyActive membrane. The experiments and modeling demonstrate that the hybrid process is more efficient than photocatalytic oxidation alone for low light irradiances. The difference in efficiency is due to a significantly higher residence time in the permeate compartment of the module than the residence time of the CSTR, respectively 20 min and 1.5 min. This allows a higher conversion of n-hexane photocatalytic oxidation associated with the constant separation capacity of the membrane, here 16.5%. However, when the kinetics of n-hexane decomposition is accelerated with the increase in light intensity absorbed by the catalyst (I_{abs}>3.5 W m^{-2}), the mass transfer process through the membrane becomes limiting (figures 8 and 10). In this case, the CSTR becomes more efficient. It is quite possible to set up a thinner membrane, a larger surface area, sweep gas or higher pressure (Figure 12) and make the hybrid process even more performant.

Moulis et al. [39] have published works describing the kinetics of n-hexane photocatalytic decomposition. For comparable operating conditions, the results of this study indicate that the reaction time to reach a removal rate of 50%-60% is about 20 min. These results are obtained with a closed loop plug flow reactor integrating a catalyst mass two times higher than the one used here and an irriadiance of 20 W m^{-2}. This also confirms the interest of coupling membrane separation and photocatalytic oxidation in the permeate compartment.

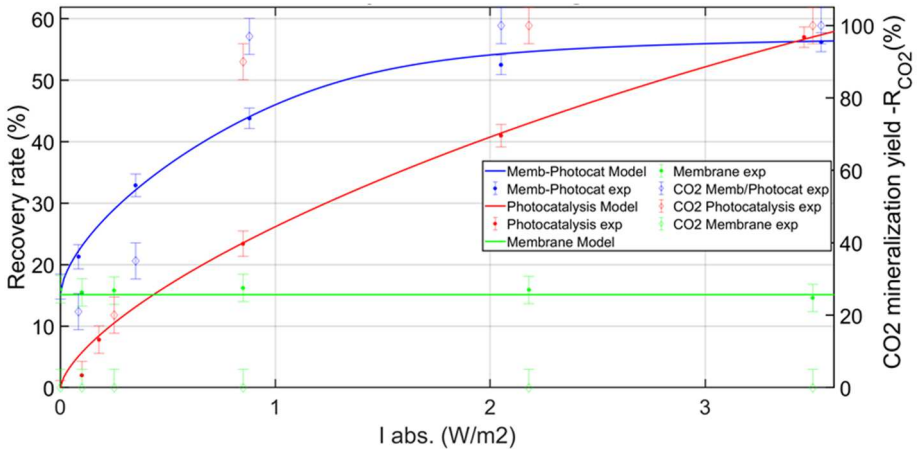

Figure 10 n-hexane recovery and mineralization ratios for three different configurations vs I_{abs} - C_{in}=10 ppm - Q_{in}=100 NmL min^{-1} - $\psi = 0.98/2$ - Catalyst *m1*

Once the progress of the photocatalytic decomposition reaction of n-hexane reaches 100%, all carbon atoms of n-hexane form carbon dioxide and the mineralization is complete. The stoichiometry of the reaction process thus corresponds to that described by equation (1). However, in some cases, photocatalytic kinetics are relatively slow and lead to partial mineralization of the compound and the formation of by-products [23, 24].

The mineralization yield of n-hexane, R_{CO2}, as a function of the absorbed light intensity is shown in Figure 10. It appears that the n-hexane flux that disappears is fully mineralized and transformed into CO_2 from I_{abs}=1 W m^{-2} for the hybrid and CSTR configurations. Below this value, a partial mineralization of the compound occurs and leads to intermediate compounds. In this case, only carbon monoxide (CO) was identified in the permeate compartment of the system and in the CSTR with concentrations of up to several hundred ppb. No presence of CO has been detected in the

retentate side. This last observation is fundamental because it indicates that the permeate compartment in which the photocatalytic oxidation occurs can constitute a by-product trap. The trap will be efficient if the permeability of an undesirable by-product is low for the membrane implemented. The concentrations of others possible by-products are lower than the detection limits of the mass spectrometer used. It is important to indicate that no reaction intermediates were detected regardless of the operating conditions applied in the study with the hybrid module. The photocatalyst showed no decrease in activity during the study and was not replaced or regenerated. However, it is highly likely that a decrease in activity will occur with the decomposition of other substances such as toluene [24].

- **Influence of the initial n-hexane concentration**

Whether it is a membrane separation process alone or coupled with a reaction process, the initial concentration of the compound of interest is an important parameter. As such, experiments have been carried out with other concentrations of n-hexane: 1, 5 and 25 ppm. Figure 11 indicates the evolution of the n-hexane recovery rate and the corresponding concentrations in the retentate and permeate compartments as a function of the light intensity absorbed by the catalyst. It appears that the lower the initial concentration of n-hexane, the lower the absorbed light intensity required to reach the maximum n-hexane recovery ratio. In other words, the lower the initial concentration, the more efficient the system is. The overall mass transfer coefficient of n-hexane does not vary over the concentration range studied, i.e. $K_{hex} \approx 3.0 \times 10^{-5}$ m s^{-1}. this means that the permeability of n-hexane is constant for the concentrations used and for the PolyActive membrane. In addition, it is important to indicate that the model proposed in this document is quite well adapted to the range of n-hexane concentration applied in the study.

(a)

(b)

(c)

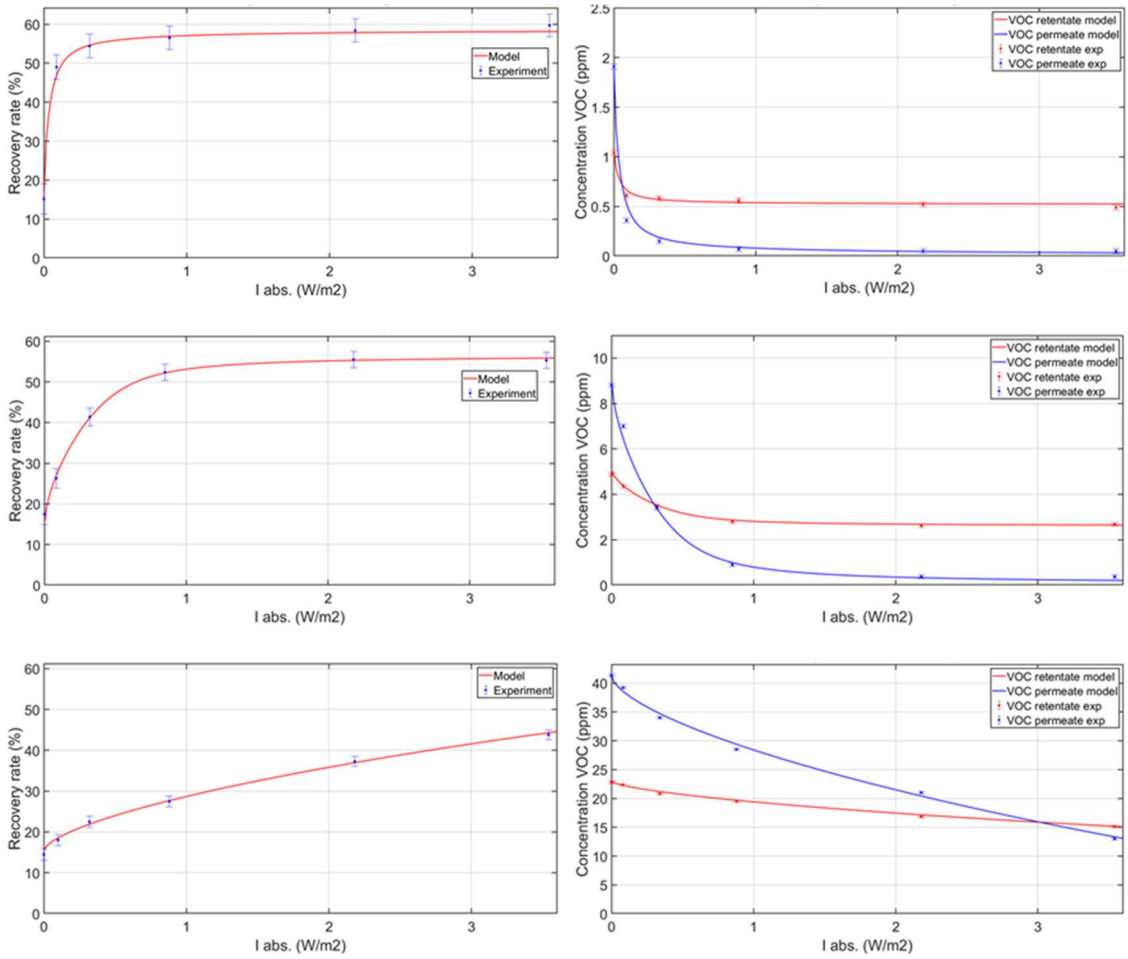

Figure 11 n-hexane recovery ratio and n-hexane retentate/permeate concentrations vs I_{abs} for C_{in}=1 ppm (a), 5 ppm (b) and 25 ppm (c) - Q_{in}=100 NmL min^{-1} - $\psi = 0.98/2$ – Catalyst *m1*

- **Influence of pressure**

The pressure level in the retentate and permeate compartments intervene directly in the transport process through the membrane of the compound of interest by acting on the driving force, i.e. by maintaining a concentration gradient on either side of the membrane. Figure 12 presents the experimental and modeled n-hexane removal rate as a function of I_{abs} for different values of ψ. For all the cases presented, we distinguish different operating regimes of the system as a function of I_{abs}: a chemical regime, a transient regime followed by a diffusive regime which becomes limiting for higher values of I_{abs}.

The results of these experiments show that for a hybrid system integrating a reaction process, the lower the I_{abs} value, the higher the n-hexane removal rate. The maximum removal rate is about 65% for ψ=0.98/3 versus 42% for ψ=0.98/1.3. However, the contribution of the reaction process to the overall n-hexane removal process is significantly higher when the value of ψ tends towards 1, since *EF* expressed according to equation (31) is about 13 for ψ=0.98/1.3 versus 1.8 for ψ=0.98/3.

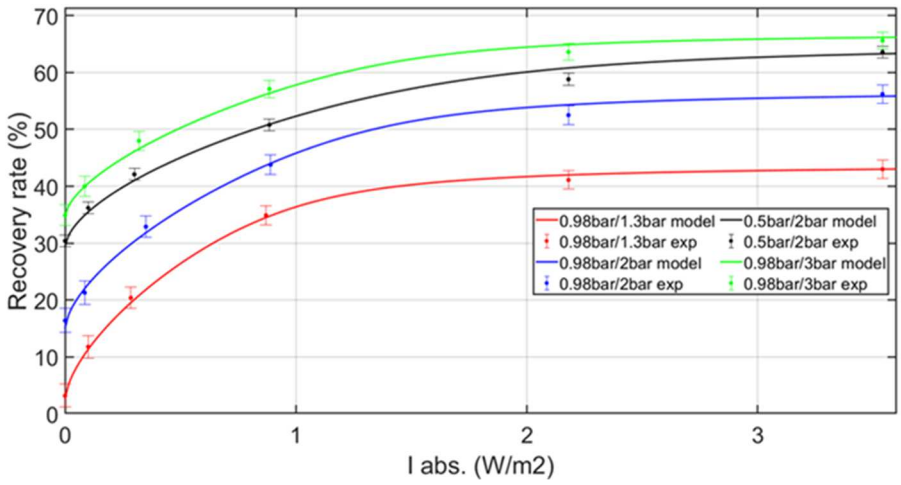

Figure 12 n-hexane recovery ratio vs I_{abs} for C_{in}=10 ppm and Q_{in}=100 NmL min^{-1} for different values of ψ- Catalyst *m1* - PolyActive Membrane

In addition, beyond lower energy consumption, the implementation of a pressure ratio ψ=0.98/1.3 leads to a low stage cut, close to 2-3% in comparison to about 18% for ψ=0.98/3 (Table 2). For the different values of ψ, the results of the modeling are consistent with the experimental results both in terms of the recovery ratio (Figure 12) and the stage cut (Table 2).

ψ	θ_{exp} (%)- (SD*)	θ_{mod} (%)
0.98/1.3	3.0 (0.2)	2.4
0.98/2	8.5 (0.3)	8.0
0.98/3	17.0 (0.2)	16.0
0.5/2	12.0 (0.2)	11.8

* Standard deviation

Table 2 Experimental and modeled stage cuts for different values of ψ- Q_{in}=100 NmL min^{-1} - PolyActive membrane

- **PDMS membrane**

The tested membrane is a 50 µm thick PDMS dense unsupported membrane. The diameter is 70 mm with an area of 38.5 cm^2. The experiments were conducted for C_{in} = 10 ppm, Q_{in} = 100 Nml min^{-1}, catalyst *m2* and for different values of ψ (Table 3). Figure 13 presents the evolution of the n-hexane removal rate as a function of the light intensity absorbed by the catalyst *m2*. Modeling was carried out with the model described in Section 2.2.1. Mass transfer coefficients were determined from the permeabilities available in the literature for each compound (Table 4) [9,41-43].

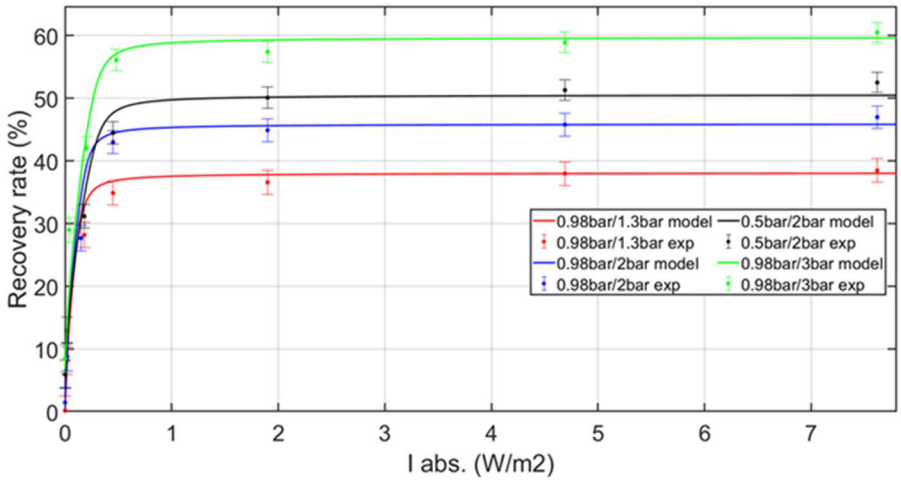

Figure 13 n-hexane recovery ratio vs I_{abs} for C_{in}=10 ppm and Q_{in}=100 NmL min^{-1} for different values of ψ- Catalyst *m2* - PDMS membrane - 50 µm

According to Figure 13, the system operates under different regimes: chemical, transient and diffusional. Comparable to the PolyActive membrane, when the catalyst *m2* is used, the diffusional regime quickly becomes the limiting regime of the overall n-hexane removal process, i.e. I_{abs}>0.2 W $m^{-2.}$ The results of these experiments indicate that, despite its thickness, the system equipped with the PDMS membrane has an n-hexane recovery ratio close to those obtained with the PolyActive membrane. The highest rate is obtained for ψ=0.98/3, i.e. 60% against about 38% for ψ=0.98/1.3. On the other hand, it also appears interesting to operate with a low stage cut e.g. close to 0.5% for ψ=0.98/1.3 (Table 3). In the latter case, the *EF* is high, about 190.

ψ	θ_{exp} (%)- (SD*)	θ_{mod} (%)
0.98/1.3	0.5 (0.1)	0.3
0.98/2	1.0 (0.1)	0.9
0.98/3	2.0 (0.2)	1.9
0.5/2	1.5 (0.2)	1.5

*Standard deviation

Table 3 Experimental and modeled stage cut for different values of ψ- Q_{in}=100 NmL min^{-1} - PDMS membrane - 50 µm

	n-Hexane	N_2	O_2	CO_2	H_20
Permeabilities (Barrer)	15000	220	450	3200	36000
K_i (m s^{-1})	$2.4x10^{-4}$	$4.2x10^{-6}$	$8.8\ x10^{-6}$	$5x10^{-5}$	$5.8x10^{-4}$

Table 4 Permeabilities and overall mass transfer coefficients for each compound

Q_{in}=100 NmL min^{-1} - PDMS Membrane - 50 µm

3.3. Modeling of a hybrid system operating in countercurrent plug flow mode

The experimental membrane module is a module the retentate and permeate compartments of which are considered to be CSTRs. This configuration does not present the highest separation yield

[5, 49]. On the other hand, a hybrid system operating in countercurrent plug flow mode, such as a hollow fiber module, should lead to significantly higher performance in terms of n-hexane removal. The modeling of this system is described in Section 2.2.2. The results of the modeling concern a hybrid module which contains a membrane consisting of a 3.5 µm thick active layer of PDMS and the catalyst $_{m1}$. The number of cells in the model is n_c=10. The feed of the module is a mixture of air and n-hexane, the concentration of which is C_{in}=10 ppm. The feed rate is Q_{in}=100 NmL min^{-1}. The photocatalyst is TiO_2 and the kinetic model is the same as the previous experimental model. The overall mass transfer coefficients for each compound are determined from the permeabilities given in Table 4.

The results presented in Figure 14 indicate that for given operating conditions, the countercurrent PF-PF system is significantly more efficient than a CSTR-CSTR system. Regardless of the light intensity used, the PF-PF system shows consistently higher n-hexane removal performance than the CSTR-CSTR system. The maximum yield difference between the two systems is observed for values close to I_{abs} = 2 W m^{-2}, while the n-hexane recovery ratio is close to 95% for the PF-PF system compared to 75% for the other system.

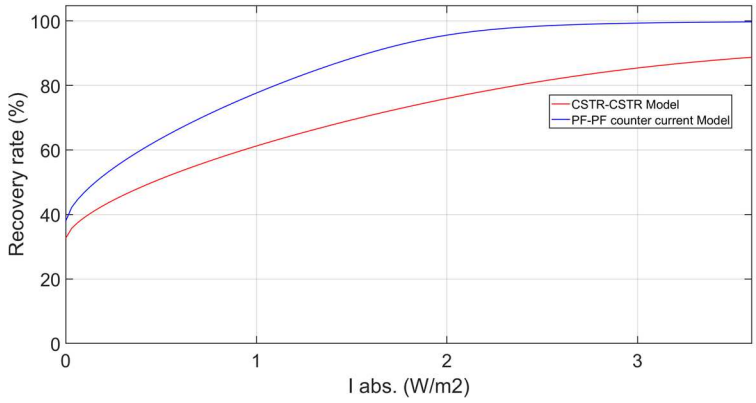

Figure 14 n-hexane recovery ratio vs I_{abs} for C_{in}=10 ppm and Q_{in}=100 NmL min^{-1} - S=60 cm^2- ψ=0.98/2- Catalyst *m1* - PDMS membrane 3.5 µm – CSTR-CSTR Model and PF-PF Model

The stage cuts corresponding to the operating conditions shown in Figure 14 are similar for both systems at 19%.

The results of coupling a membrane separation process and a reaction process such as the one presented in this study can obviously lead to an interpretation that is based on two points of view.

First, this hybrid process can be considered as a process of intensification of VOC membrane separation. The hybrid system operating in countercurrent PF mode makes it possible to obtain, even for very low concentrations, high n-hexane recovery ratios for low values of ψ and I_{abs}, e.g. ψ=0.98/1.3, and for I_{abs} ≈3 W m^{-2} (Figure 15a). The membrane surface area ranges from 30 to 180 cm^2 with the corresponding stage cuts ranging from 3 to 18%. The efficiency of the system can be significantly increased by supplying the module with a sweep gas on the permeate side (Figure 15b). With a sweep gas flow rate Q_{sw} corresponding to 30% of Q*in* and X_{sw}=0, the system will be very efficient even at I_{abs} values of less than 3 W m^{-2}.

For S=60 cm^2, θ=6% and I_{abs} = 3 W m^{-2}, the n-hexane removal efficiency is 90% and the flow rate on the retentate side is 94 NmL min^{-1}. For this case, *EF* is 11. To obtain similar results, a countercurrent PF-PF membrane module with equivalent characteristics but without coupling can operate either with vacuum pumping on the permeate side or with feed compression. Thus, the first configuration is that the module operates either with a feed flow rate of 115 NmL min^{-1}, ψ=0.18/1.3 and θ=20%. The second configuration is a feed flow rate of 142 NmL min^{-1}, ψ=0.98/3.3 and θ=32%.

The power P_{Total} (W) required for the operating system is estimated from equations (33) and (34).

$$P_{Total} = P_{Comp} + P_{vac} + P_{Light} \qquad (33)$$

P_{comp} (W) and P_{vac} (W) are the compressor power and the vacuum pump power respectively. These powers are calculated with Memsic© software, based on classical compressors and vacuum pumps energy requirement expressions [48,49]. P_{Light} (W) is the light power absorbed by the catalyst.

$$P_{Light} = \frac{I_{abs}}{E_{light}} \times S_{cat} \qquad (34)$$

E_{light} represents the energy efficiency of the light source. In this study, the E_{Light} of the LEDs used is about 0.3. S_{cat} is the illuminated catalyst surface area, here for the catalyst *m1*, S_{cat}=38.5 cm^2.

For the configurations shown above, the total power requirements are:

- Hybrid countercurrent PF-PF module, ψ=0.98/1.3 - I_{abs}≈3 W m^{-2}

$$P_{Total} = P_{Comp} + P_{vac} + P_{Light} = 63 \times 10^{-3} + 0 + \left(\frac{3}{0.3}\right) \times 38.5 \times 10^{-4} = 0.101W$$

- Simple countercurrent PF-PF module, ψ=0.18/1.3 – I_{abs}=0 W m^{-2}

$$P_{Total} = P_{Comp} + P_{vac} + P_{Light} = 75 \times 10^{-3} + 125 + 0 = 0.200W$$

- Simple countercurrent PF-PF module, ψ=0.98/3.3 – I_{abs}=0 W m^{-2}

$$P_{Total} = P_{Comp} + P_{vac} + P_{Light} = 485 \times 10^{-3} + 0 + 0 = 0.485W$$

For a similar n-hexane recovery ratio, the hybrid countercurrent PF-PF system is particularly advantageous from an energy point of view compared to a simple PF-PF membrane module. The power requirement is reduced by a factor of two compared to vacuum configuration, which is known to offer the best energy efficiency for membrane gas separations [49]. The interest of the photodriven concept for achieving high energy efficiency, as suggested in the introduction section, is thus confirmed. Besides the economy for operating expenses (OPEX), it should be stressed that no capital cost (CAPEX) for vacuum pump is needed. A cheap diode light source can be used, offering interesting performances in terms of compactness, compared to a classical compression or vacuum pumping process. It is important to mention that it is possible to improve this energy gain with the use of a direct or indirect solar light source [50] and achieve an energy gain of 3.2. This factor can reach 7.7 for the feed compression solution and a solar source. Such a simplified analysis would suggest the systematic application of a vacuum pumping strategy, in order to minimize the energy requirement of the process. Industrial feedback shows that this option is very rarely chosen in particular because of the difficulty of achieving vacuum at an industrial scale [49].

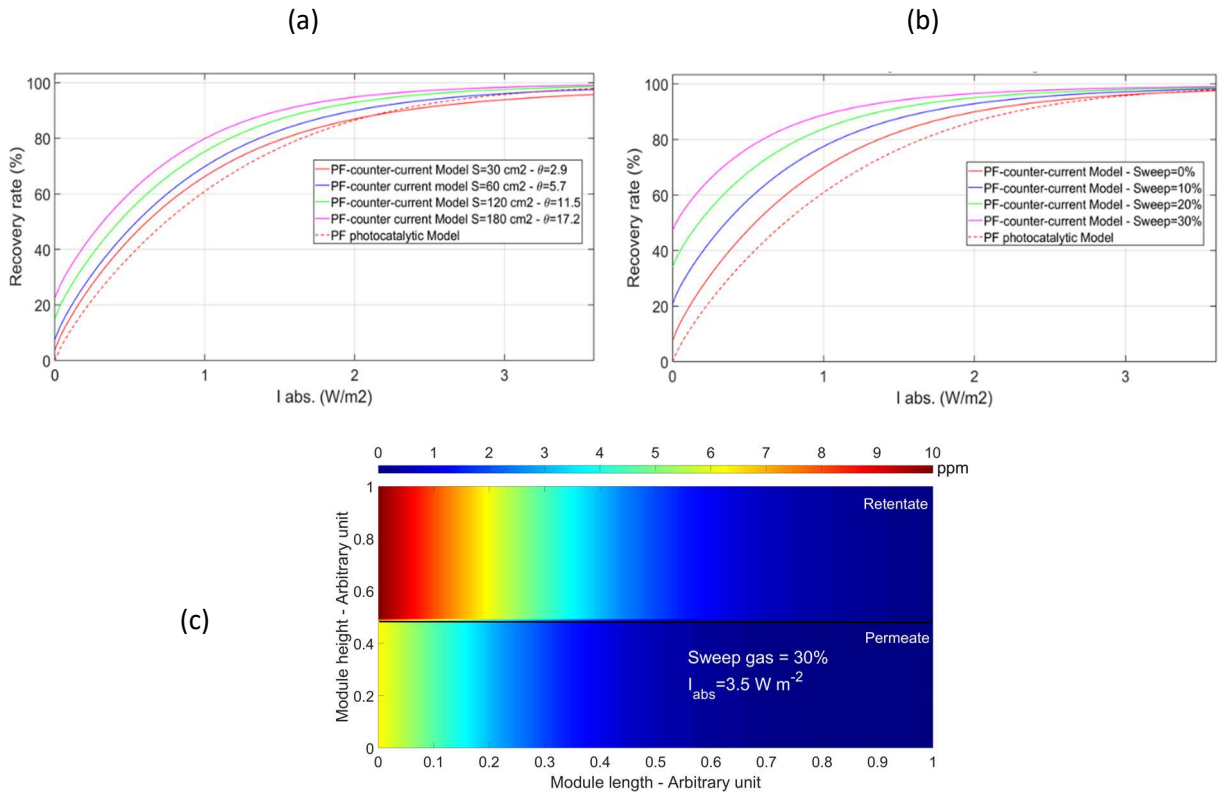

Figure 15 n-hexane recovery ratio vs I_{abs} for different surface areas (a), sweep gas flow rate (b) and evolution of n-hexane concentrations in the module (c) - C_{in}=10 ppm and Q_{in}=100 NmL min^{-1} - S=60 cm^2- ψ=0.98/1.3- Catalyst *m1* - PDMS membrane - 3.5 µm – countercurrent PF-PF Model

The interpretation of the modeling results presented can also be conducted from a second point of view: that of the intensification of a reaction process. In some situations, such as the remediation of indoor air containing VOCs, the aim is to decompose a pollutant. The use of photocatalytic reactors is relatively widespread [15-17,22,51,52]. Numerous studies indicate that the most efficient configuration of operation of these reactors is the plug flow mode [17,22, 52].

The recovery ratio of n-hexane obtained by modeling with the equation (31) for a photocatalytic plug flow reactor is shown in Figure 15. The catalyst mass is *m1*=0.150 g, the feed rate Q_{in} =100 NmL min^{-1} and the reactor pressure is 0.98 bar. The kinetic model of n-hexane decomposition is the one applied previously.

Under the operating conditions used in this part of the study, the hybrid module appears to be more efficient than a photocatalytic plug flow reactor in main configurations (Figure 15). The differences in

terms of n-hexane removal rates can be high between the two systems when the module is fed with a sweep gas flow rate on the permeate side and for I_{abs}<3 W m^{-2}. As for the CSTR configurations, the difference is explained by a higher residence time in the permeate compartment of the hybrid module than the residence time in the photocatalytic plug flow reactor. This phenomenon is enhanced by the separation property of the membrane. Furthermore, the counter-current configuration also improves the performance of the hybrid process by maintaining a relatively constant driving force between the retentate and permeate compartments (figure 15c).

However, with ψ=0.98/1.3, the energy cost will be slightly unfavorable to the hybrid module if a direct solar source is not used. Modeling indicates that it is possible to maintain a high n-hexane recovery ratio with a hybrid module operating with ψ≈1 and sweep gas flow rate.

4. Conclusion

The work presented in this paper focuses on the coupling of gas permeation using a dense polymeric membrane and a photocatalytic process placed in the permeation compartment of a membrane module. The initial aim of the study is to demonstrate the ability of such a separation technique to remove low-concentration n-hexane from air.

The results of this work show that the hybrid device allows significant intensification of the membrane separation of n-hexane from air for very low concentrations, up to 1 ppm. The n-hexane mineralization can be complete with a light source that exposes the catalyst to a UV-A irradiance of a few W m^{-2}. Under the experimental conditions of the study, no by-products other than water and carbon dioxide were detected.

From an energy point of view, the combination of a membrane technology and an oxidation process such as photocatalysis is of great interest. For n-hexane, it has been demonstrated that a hybrid system can lead to a significant reduction in the power required to achieve high removal efficiencies. Moreover, the study reveals that coupling of these two processes can also be very efficient from a reaction point of view. Indeed, for similar operating conditions, a hybrid system operating in

countercurrent plug flow mode will show performance that can be much higher than a photocatalytic plug flow reactor. The implementation of an advanced oxidation process in the permeate compartment of the system could be also an opportunity to reduce the presence in the treated effluent of by-products potentially formed during the photocatalytic decomposition of VOCs. Indeed, the relatively long residence time in the permeate compartment should contribute to higher rates of mineralization. Moreover, the residual by-products could also be trapped more or less efficiently in the permeate compartment according to their respective permeability and operating conditions. It might be that the membrane photodriven technology explored in this study, which operates under continuous regime, does not requires a regeneration step, and is not sensitive to humidity, becomes a relevant alternative to adsorption for trace VOC removal. To that respect, further experiments will be performed on different VOC compounds more toxic than n-hexane, such as toluene and formaldehyde, to show the generic applicability of the process.

More generally, the promising results of this study suggest to extend the concept to integrated membrane systems operating with a direct or indirect solar light source. The applications for these combined separation / reaction systems are numerous, for indoor air treatment or for the purification of industrial or medical gases.

References

[1] F.I. Khan, A. Kr. Ghoshal, Removal of Volatile Organic Compounds from polluted air. J. Loss. Prev. Process. Ind. 13 (2000) 527–545

[2] F. Salvador, N. Martin-Sanchez, R. Sanchez-Hernandez, M.J. Sanchez-Montero, C. Izquierdo,. Regeneration of carbonaceous adsorbents. Part I: thermal regeneration, Micropor. Mesopor. Mat. 202 (2015) 259–276.

[3] H. Abiko, M. Furuse, T. Takano, Reduction of adsorption capacity of coconut shell activated carbon for organic vapors due to moisture contents, Ind. Health 48 (2010) 427–437.

[4] L. Jia, J. Shi, C. Long, F. Lian, B. Xing, VOCs adsorption on activated carbon with initial water vapor contents: Adsorption mechanism and modified characteristic curves, Sci. Total Environ. 731 (2020) 139184.

[5] R.W. Baker, Membrane Technology and Applications, John Wiley & Sons, 2004.

[6] J.S. Cha, V. Mailik, D. Bhaumik, R. Li, K.K. Sirkar, Removal of VOCs from waste gas stream by permeation in a hollow fiber permeator, J. Membr. Sci. 128 (1997) 195–211.

[7] D. Bhaumik, S. Majumdar, K.K. Sirkar, Pilot-plant and laboratory studies on vapor permeation removal of VOCs from waste gas using silicone-coated hollow fibers, J. Membr. Sci. 167 (2000) 107-122.

[8] Y. Liu, X. Feng, D. Lawless, Separation of gasoline vapor from nitrogen by hollow fiber composite membranes for VOC emission control, J. Membr. Sci. 271 (2006) 114–124.

[9] Z. Petrusová, K. Machanová, P. Stanovský, P. Izák, Separation of organic compounds from gaseous mixtures by vapor permeation, Sep. Purif. Technol. 217 (2019) 95–107

[10] L.M. Sun, J.Y. Thonnelier, Perméation gazeuse – Techniques de l'ingénieur [J2810 V1], 2004.

[11] S. Majumdar, D. Bhaumik, K.K. Sirkar, Performance of commercial-size plasmapolymerized PDMS-coated hollow fiber modules in removing VOCs from N2/air, J.Membr. Sci. 214 (2014) 323–330.

[12] R.G. Rebollar-Perez, E. Carretier, N. Lesage, P. Moulin, Vapour permeation of VOC emitted from petroleum activities: Application for low concentrations, J. Ind. Eng. Chem. 18 (2012) 1339–1352

[13] W. Rongwong, S. Boributh, S. Assabumrungrat, N. Navadol Laosiripojana, R. Jiraratananon, Simultaneous absorption of CO2 and H2S from biogas by capillary membrane contactor, J. Membr. Sci. 392 - 393 (2012) 38– 47.

[14] R.M. Alberici; W.F Jardim, Photocatalytic destruction of VOCs in the gas-phase using titanium dioxide, Appl. Catal. B 14 (1997) 55 − 68.

[15] F. Gérardin, A. Cloteaux, M. Guillemot, M. Faure, J.C. André, Photocatalytic conversion of gaseous nitrogen trichloride into available chlorine—experimental and modeling study. Environ. Sci. Technol. 47 (2013) 4628-4635.

[16] A. Cloteaux, F. Gérardin, D. Thomas, N. Midoux, J.C. André, Fixed bed photocatalytic reactor for formaldehyde degradation: Experimental and modeling study, Chem. Eng. J. 249 (2014) 121-129.

[17] Y. Boyjoo, H. Sun, J. Liu,V.K. Pareek, S. Wang, A review on photocatalysis for air treatment: From catalyst development to reactor design, Chemical Engineering Journal 310 (2017) 537–559.

[18] D. Wood, S. Shaw, T.Cawte, E. Shanen, B. Van Heyst, An overview of photocatalyst immobilization methods for air pollution remediation. Chem. Eng. J. 391 (2020) 123490.

[19] M. Jędrzejczyk, K. Zbudniewek, J. Rynkowski, V. Keller, J. Grams, A.M. Ruppert, N. Keller, Wide band gap Ga2O3 as efficient UV-C photocatalyst for gas-phase degradation applications, Environ Sci. Pollut. Res. 24 (2017) 26792–26805.

[20] Y. Huang, H. Hu, S. Wang, M.S. Balogun, H. Ji, Y. Tong, Low concentration nitric acid facilitate rapid electron–hole separation in vacancy-rich bismuth oxyiodide for photo-thermo-synergistic oxidation of formaldehyde. Appl. Catal. B-Environ. 218 (2017), 700–708.

[21] Y. Huang, Z. Guo, H. Liu, S. Zhang, P. Wang, J. Lu, Y. Tong, Heterojunction Architecture of N-Doped WO_3 Nanobundles with Ce_2S_3 Nanodots Hybridized on a Carbon Textile Enables a Highly Efficient Flexible Photocatalyst. Adv. Funct. Mater. 29 (2019) 1903490.

[22] K. Vikrant, C.M. Park, K.H. Kim, S. Kumar, E. C. Jeon, Recent advancements in photocatalyst-based platforms for the destruction of gaseous benzene: Performance evaluation of different modes of photocatalytic operations and against adsorption techniques. J. Photochem. Photobiol. C 41 (2019) 100316.

[23] F. He, U. Muliane, S. Weon, W. Choi, Substrate-specific mineralization and deactivation behaviors of TiO_2 as an air-cleaning photocatalyst, Appl. Catal. B-Environ. 275 (2020) 119-145.

[24] M. Le Bechec, N. Kinadjian, D. Ollis, R. Backov, S. Lacombe, Comparison of kinetics of acetone, heptane and toluene photocatalytic mineralization over TiO_2 microfibers and Quartzel® mats, Appl. Catal. B-Environ. 179 (2015) 78–87.

[25] K. Sirkar, P. Shanbhag, A. Kovvali, Membrane in a reactor: a functional perspective, Ind. Eng. Chem. Res., 38 (10) (1999) 3715–3737.

[26] S.J.G. Sanchez, S. Marcano, T.T. Tsotsis, Catalytic membranes and membrane reactors, Wiley-VCH, Weinheim, 2002.

[27] T. Westermann, T. Melin, Flow-through catalytic membrane reactors—Principles and applications, Chem. Eng. Process. 48 (2009) 17–28.

[28] E. Bet-moushoul, Y. Mansourpanah, K. Farhadi, M. Tabatabaei, TiO2 nanocomposite based polymeric membranes: A review on performance improvement for various applications in chemical engineering processes, Chem. Eng. J. 283 (2016) 29–46.

[29] W. Qing, X. Li, S. Shaob, X. Shi, J.Wang, Y. Feng, Polymeric catalytically active membranes for reaction-separation coupling: A review, J. Membr. Sci., 583 (2019) 118–138.

[30] S. Leong, A. Razmjou, K. Wang, K. Hapgood, X. Zhang, H. Wang, TiO2 based photocatalytic membranes: a review, J. Membr. Sci. 472 (2014) 167–184.

[31] J. Su, Yang, C. Cheng, C. Huang, H. Xu, Q. Ke, Hierarchically structured TiO2/PAN nanofibrous membranes for high-efficiency air filtration and toluene degradation, J. Colloid Interface Sci. 507 (2017) 386–396.

[32] T. Tsuru, T. Toyosada, T. Yoshioka, M. Asaeda, Photocatalytic reactions in a filtration system through porous titanium dioxide membranes, J. Chem. Eng. Jpn. 34 (2001) 844.

[33] G. Camera-Roda, V. Loddo, L. Palmisano, F. Parrino, F. Santarelli, Process intensification in a photocatalytic membrane reactor: Analysis of the techniques to integrate reaction and separation, Chem. Eng. J. 310- 2 (2017) 352-359.

[34] T. Tsuru, T. Kan-no, T. Yoshioka, M. Asaeda M., A photocatalytic membrane reactor for gas-phase reactions using porous titanium oxide membranes, Catal. Today 82 (1–4) (2003) 41–48.

[35] T. Tsuru, T. Kan-no, T. Yoshioka, M. Asaeda, A photocatalytic membrane reactor for VOC decomposition using Pt-modified titanium oxide porous membranes, J. Membr. Sci. 280 (2006) 156–162.

[36] A.J. Maira, W.N. Lau, C.Y. Lee, P.L. Yue, C.K. Chan, K.L. Yeung, Performance of a membrane-catalyst for photocatalytic oxidation of volatile organic compounds, Chem. Eng. Sci., 58 (2003) 959-62.

[37] J. Liu, S. Wang, T. Huang, P. Manchanda, E.A. Hamad, S.P. Nunes, Smart covalent organic networks with on-off-on light switchable pores for molecular separations, Science Advances 6 (2020) 1-11.

[38] G. Van der Veen, W. Prins, Photomechanical energy conversion in a polymer membrane, Nature 230 (1971), 70-720.

[39] F. Moulis, J. Krýsa, Photocatalytic degradation of several VOCs (n-hexane, n-butyl acetate and toluene) on TiO2 layer in a closed-loop reactor, Catal. Today 209 (2013) 153–158.

[40] C.J. Bueno-Alejo, J.L. Hueso, R. Mallada, I. Julian, J. Santamaria, High-radiance LED-driven fluidized bed photoreactor for the complete oxidation of n-hexane in air. Chem. Eng. J. 358 (2019) 1363–1370.

[41]E. Favre, P. Schaetzel, Q.T. Nguygen, R. Clément, J. Néel, Sorption, diffusion and vapor permeation of various penetrants through dense poly(dimethylsiloxane) membranes: a transport analysis, J. Membr. Sci. 92 (1994) 169.

[42] C.K. Yeom, S.H. Lee, H.Y. Song, J.M. Lee, Vapor permeations of a series of VOCs/N2 mixtures through PDMS membrane, J. Membr. Sci. 198 (2002) 129–143.

[43] L.Z. Zhang, X.R. Zhang, Q.Z. Miao., L.X. Pei, Selective permeation of moisture and VOCs through polymer membranes used in total heat exchangers for indoor air ventilation, Indoor Air 22 (2012) 321–330.

[44] K. Schuldt, J. Pohlmann, S. Shishatskiy, T. Brinkmann, Applicability of PolyActive™ Thin Film Composite Membranes for CO2 Separation from C2H4 Containing Multi-Component Gas Mixtures at Pressures up to 30 Bar, Membranes 8 (2018) 27.

[45] P. Bernardo, E. Drioli, G. Golemme, Membrane Gas Separation: A Review/State of the Art. Ind. Eng. Chem. Res. 48 (2009) 4638–4663.

[46] E. Fehlberg, “Low-order Classical Runge-Kutta Formulas with Stepsize Control.” NASA Technical Report R-315, 1969.

[47] A. Makaruk, M. Harasek, Numerical algorithm for modelling multicomponent multipermeator systems, J. Membr. Sci. 344 (1–2) (2009) 258–265.

[48] R. Bounaceur, E. Berger, M. Pfister, A.A. Ramirez Santos, E. Favre, Rigorous variable permeability modelling and process simulation for the design of polymeric membrane gas separation units: MEMSIC simulation tool, J. Membr. Sci. 523 (2017) 77–91.

[49]E. Favre, Polymeric Membranes for Gas Separation. In: Enrico Drioli and Lidietta Giorno, Comprehensive Membrane Science and Engineering, volume 2, pp. 155–212 Oxford: Academic Press. 2010.

[50] M. Romero, J.N. Blanco, B.S. Nchez, A. Vidal, A.I. Cardona, E. Garcia, solar photocatalytic Degradation of Water and Air Pollutants: challenges and Perspectives, Solar Energy 66 (2) (1999) 169–182.

[51] O. Debono , V. Hequet , L. Le Coq , N. Locoge , F. Thevenet, VOC ternary mixture effect on ppb level photocatalytic oxidation: Removal kinetic, reaction intermediates and mineralization, Appl. Catal. B-Environ. 218 (2017), 359-369.

[52] B.M. da Costa Filho, V.J.P. Vilar, Strategies for the intensification of photocatalytic oxidation processes towards air streams decontamination: A review. Chem. Eng. J. 391 (2020) , 123531.

Graphical abstract